ISSN 0554-6397
Prethodno priopćenje
(*Preliminary communication*)

Darin Majnarić
E-mail: dmajnaric@riteh.hr
Albert Zamarin
E-mail: zamarin@riteh.hr
University of Rijeka, Faculty of Engineering
Vukovarska 58, 51000 Rijeka, Croatia

Stiffness Adjustment of Surface-Piercing Hydrofoils Within Fluid-Structure Interaction

Abstract

This paper presents results from numerical analysis of the fluid and structure interaction of two different hydrofoil models, Model 1 and Model 2. Analyzes were performed with stainless steel, aluminium and composite materials for Model 1, and Model 2 was created from composite with aluminium reinforcement. Models were analyzed for three different angles of attack (10, 20, 30 degrees) and for each angle three different speeds were tested (2, 4, 6 m/s). At first, the whole set of analysis was run for entirely submerged hydrofoils and later on for immersed hydrofoils to the draft *h*. Described numerical analysis was performed in order to adjust stiffens of hydrofoils based on different operational loads. Two-way fluid-structure interaction analysis was used which combines FEM and CFD solvers. Presented results are based on 44 analysis with which all planned conditions of hydrofoil operation were tested. Numerical analysis showed a correlation between stiffens of material i.e. structural response and hydrodynamic loading. Besides mentioned, based on analysis of Model 2 future prediction are given in a way of hydrofoil design or particularly placement for hydrofoils reinforcement.

Keywords: FSI, hydrofoils, stiffness adjustment, composite

1. Introduction

In recent years hydrofoils are again getting momentum in usage given the development of high-speed foiling yachts, high-speed passengers ships, hydrofoil motor yachts, and even new surfing boards. At the same time with the increased hydrofoil usage goes development of numerical analysis software's which with one-way and two-way fluid-structure interaction [1, 2] are able to get significantly close to experimental methods [3, 4, 5]. Beside mentioned uprising of composite materials especially in aero and shipbuilding industry has a major impact on usage and future development of stronger hydrofoils and other ship parts. Currently, application of composite materials in hydrofoils is major topic that is still in progress and it is following development of

composite materials. Significant progress is made in experimental studies of hydrofoils [6, 7, 8] and comparison between experimental and numerical results [9, 10].

This paper meets some points in still-open questions like application and verification of two-way fluid-structure interaction, composite usage in hydrofoil construction and stiffens adjustment. Verification of two-way fluid-structure interaction method is done by help of *ANSYS* softer package [11] based on the comparison of obtained results and known physical behavior of hydrofoils. For verification of used previously described method, a decision was made to start research with stainless steel as most robust material used in development of hydrofoils. Behavior analysis of aluminium and composite materials was used for stiffness adjustment with focus on composite material for which second model was created. Mentioned setup directions are described in detail in second chapter named *Numerical setup and modeling techniques*. The main contribution of this paper can be found in third chapter *Results and discussion* in which results are presented for behavior of composite hydrofoil in different load situations along with impact of inserted stiffener on general hydrofoil stiffness. Mentioned results of composite material analysis are highlighted among results presented also for behavior of hydrofoils with material properties of aluminium and stainless steel. Obtained results can be used when considering material properties for hydrofoil design based on expected operational loads. Fourth and final chapter "Conclusion" contains summary of achieved results and impact that this paper represents for current knowledge of hydrofoil behavior and for future studies on the topic.

2. Numerical setup and modeling techniques

For the purpose of numerical analysis and in order to define structure domain two different 3D hydrofoil geometries were created. Models were marked as Model 1 and Model 2 because of easier identification. Both models have the same basic geometrical shape and dimensions, primary hydrofoil model geometry can be seen in Figure 1 left, which is a representation of Model 1. The only difference between Model 1 and Model 2 is additional geometry on the back of Model 2 that represent stiffener geometry. Additional geometry is marked with an arrow in Figure 1 right, that is a representation of Model 2.

As shown in Figure 1. basic geometrical dimensions are; height $S = 91$ cm, length of the cross-section C=27.94 cm, profile thickness $T = 2.79$ cm, a circular arc (ogival) forebody with a radius of curvature 85 cm, and a rectangular after-body. The section has a leading-edge radius of $0.01C$ (0.28 cm) and a blunt trailing edge. The described geometrical model was used in past studies with similar or identical dimensions [9, 12, 13, 14, 15]. Based on past studies it was easier to validate results and research method. Difference from described basic geometry is an addition in length of a chord that can be seen on Model 2, Figure 1 right, C=27.94 + 0.6 cm [9].

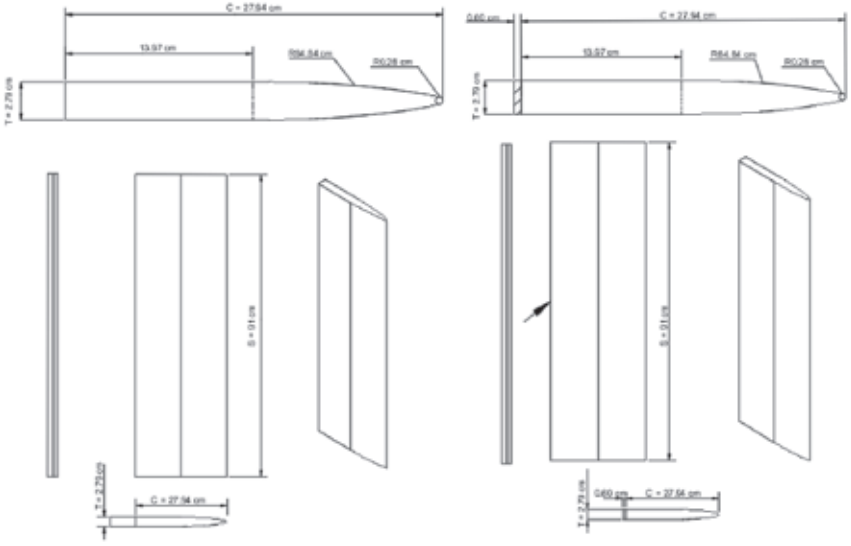

Figure 1: Dimensions of Model 1 (left), and dimensions of Model 2 (right)

Two models of hydrofoils were tested with the usage of different material properties. Selected materials for this research were stainless steel, aluminium alloy, and composite. Analysis with Model 1 was carried out for all three different materials, as for Model 2 only composite material properties were used for the main body that was combined with an aluminium alloy which was used only as an additional stiffener. Model 1 was divided into three different models depending on the material used in each of them, namely Model1a for stainless steel, Model1b for aluminium alloy and Model1c for composite material. Material properties for stainless steel and aluminium are presented in Table 1 and the material properties of composite material are presented in Table 2.

Table 1: Material properties for aluminium and stainless steel

Mechanical properties	Aluminium	Stainless steel
Density, kg/m^3	2770	7850
Young's modulus *E*, GPa	71	200
Shear modulus *G*, GPa	26	77
Poisson's ratio, *v*	0,33	0,3

Table 2: Material properties for composite material, carbon epoxy (unidirect.) [16]

Mechanical properties	Composite
Density, kg/m^3	1500
Young's modulus Ex, MPa	38700
Young's modulus Ey, MPa	6500
Young's modulus Ez, MPa	6500
Poisson's ratio, v_{xy}	0,35
Poisson's ratio, v_{yz}	0,34
Poisson's ratio, v_{xz}	0,059
Shear modulus Gxy, MPa	1700
Shear modulus Gyz, MPa	2400
Shear modulus Gxz, MPa	1700

Structure domain is defined if the software has information about material properties of the structure and its geometry. To define other crucial information as orientation in space and boundary conditions, first fluid domain needs to be defined. For the purpose of this analysis, the fluid domain was defined in accordance with recommendations of ITTC (*International towing tank conference*) [17]. Dimensions of fluid domain were defined as a function of the length (*S*) of the structural model in a way in which borders are distanced from. Consequently, lengths were set as $0.5 \cdot S$ in front of the structural model, $2.5 \cdot S$ back of the model, $0.75 \cdot S$ length to the bottom, $0.5 \cdot S$ to the top and $1.25 \cdot S$ was length to the right and left of the model, [18]. Also, with described dimensions the mutual position of structural domain and fluid domain was given. Given dimensions of fluid domain were used as initial values, where final domain borders were determined based on additional 15 conducted simulations. Those simulations were done in order to optimize fluid domain borders for particular research. Optimization of fluid domain dimensions was the iteration process in which borders size were reduced with which numerical simulation time was minimized and in the same time simulation results remain in satisfactory limits. Final fluid domain boundaries were changed for space behind and for space beside structural model to $2.25 \cdot S$ back of the model and $0.5 \cdot S$ to the left and right of the model.

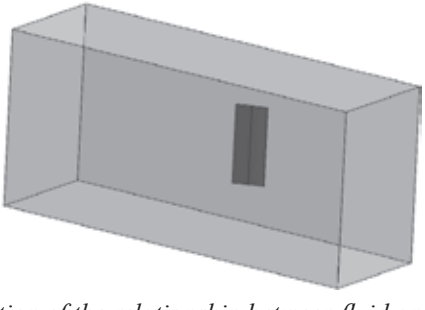

Figure 2: Representation of the relationship between fluid and structure domain in space

The analysis was carried out within *ANSYS* software [11] through two-way fluid-structure interaction analysis with module *SYSTEM COUPLING* which was used for coupling *FEM* and *CFD*. For structural domain (*FEM*) [14] *TRANSIENT STRUCTURAL* module in which *ANSYS* mechanical APDL solver was used and for the fluid domain (*CFD*) *FLUID FLOW* module was used. Both of mentioned solvers are integrated within *ANSYS* software package and with these three modules full two-way fluid-structure interaction (*FSI*) can be performed. Two-way *FSI* interaction is basically working on iteration process in which in each step structural and fluid solver are exchanging information about mutual mesh deformations.

TRANSIENT STRUCTURAL was used to set up hydrofoil domain mesh and *FEM* solver, while *FLUID FLOW* module was used to set up fluid domain mesh, and *CFD* solver in which variables like attack angle and Reynolds number were modified. In *SYSTEM COUPLING* module simulation end time was set to 25 seconds with time step of 0.01 seconds. Maximum number of iterations was set to 25. In each step the simulation forces from *CFD* solver were transported into *FEM* solver and deformations from *FEM* were transported to *CFD* solver.

Before the launch of coupling analysis structure and fluid meshes were defined. The decision was made to use tetrahedral mesh type because it was the most appropriate type regarding the ratio of mesh quality and the number of elements in the model. A point worth of mentioning is that in this numerical experiment, consisting of 44 analysis it was important to find optimal line between time that is needed for each analysis and mesh quality that can produce validate results. As can be seen in Figure 3. left, mesh of structural domain is presented, and on Figure 3. right mesh quality can be seen with element quality legend in which max value represents the highest quality and min value represents worst quality elements based on aspect ratio criteria.

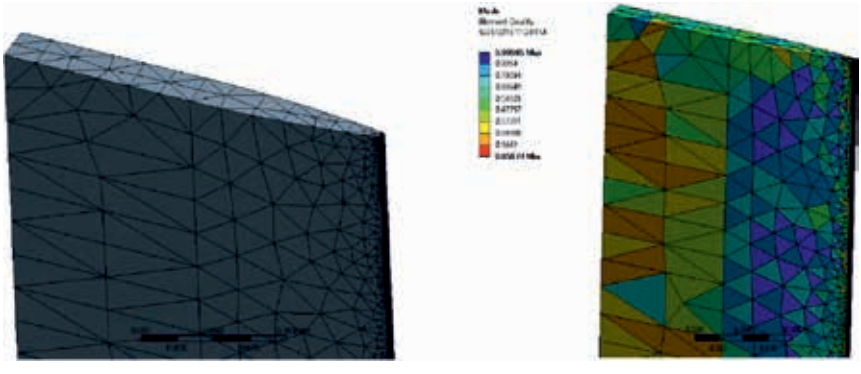

Figure 3: Representation of generated mesh for structural domain (left), and representation of mesh quality (right)

Models of hydrofoils created for the structural domain were fixed in all cases with one boundary condition in which the top surface of the structure model was fixed in all six degrees of freedom.

Based on structural domain fluid domain was created and its mesh was adjusted to the same element quality of structural mesh in order to preform coupled analysis. Special attention was given to the area around the hydrofoil entry edge, Figure 4, where element size was reduced in order to get better mesh quality and consequently more accurate results. Also due to motion of boundaries during the simulation dynamic mesh was defined.

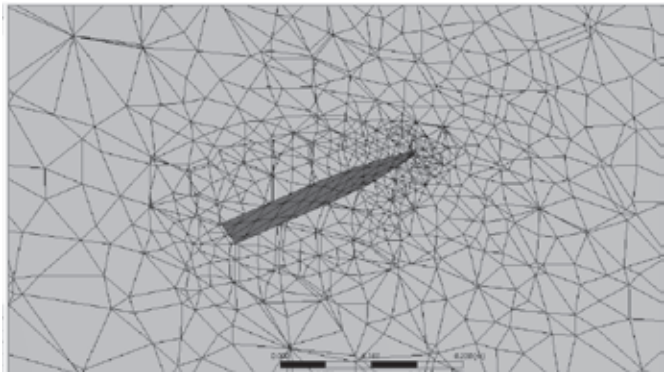

Figure 4: Representation of mesh elements of fluid domain around the structure domain area

All boundary conditions for fluid domain were set as walls except front and back (*x*-axis on Figure 5.) of domain defined as inlet and outlet. The flow was set in the opposite direction of *x*-axis, Figure 5, starting with inlet and ending with outlet. Fluid for the fluid domain was set as water.

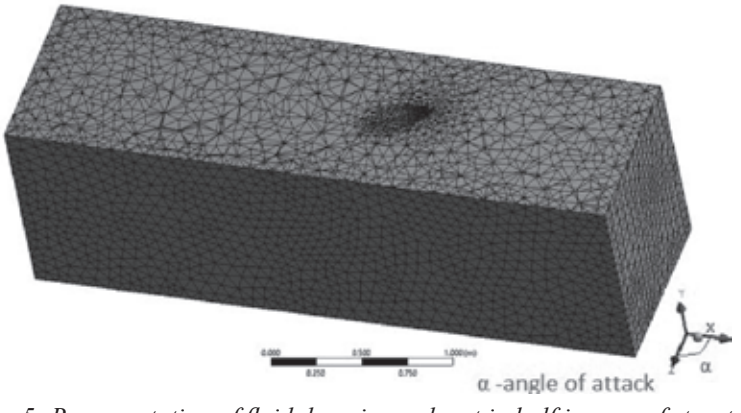

Figure 5: Representation of fluid domain mesh cut in half in area of structural domain

Conducted numerical simulations were depending on various physical values that were controlled with input data, some of them are shown within Table 3. Main values that were different for each simulation were inflow speed of water and angle of attack in combination with used materials. Three values of inflow speed were used which were speeds of 2, 4 and 6 m/s. For angle of attack which defines the angle of water inflow on hydrofoil, also was modified between three different values of 10, 20, 30 degrees. Negative x-axis water inflow was set, Figure 5, and angle of attack of hydrofoil was changed in accordance with the *xy* plane. All simulations were performed for two different immersed values of tested models. The first set of simulations were carried out for model draft of 35 cm (*h*), and the second set of simulations for fully immersed models. Simulations standards were set with values presented in Table 3. [9].

Table 3: Values of experiment conditions

Immersion of hydrofoil	h	0,35 - 0,91	m
Immersion 'Aspec ratio'	$AR_h=h/C$	0,38 - 1,0	-
Velocity	u	2 - 6	m/s
Depth Froude number	$Fn_h=u\cdot\sqrt{gh}$	0,5 - 5,0	-
Reynolds number	$Re_c=uC/v$	$1.5 10^5$ - $1,7\cdot10^6$	-
Attack angle	α	10 - 30	°

Immersion of profile value was defined with symbol *h* and operating limits were from 0.35 cm to 0.91 cm. Second value was immersed "Aspect ratio" where *h* defines the height of immersed hydrofoil part and *C* stands for chord length of circuits body. The ratio of *h* and *C* was calculated by the formula:

$$AR_h = \frac{h}{C} \tag{1}$$

Next variable was Froude number (depth);

$$Fn_h = \frac{u}{\sqrt{gh}} \tag{2}$$

In which *g* was gravitational acceleration, *h* defines the height of immersed hydrofoil part and was velocity. The formula was used as an indication of ratio between pressure level along model and pressure gradient along chord length.

By Reynolds number fluid flow state can be determined between the laminar and turbulent flow.

$$Re_c = \frac{uC}{v} \tag{3}$$

Where *u* was the fastest fluid flow speed, *C* chord length of circuits body and *v* was fluid kinematic viscosity.

3. Results and discussion

The results are presented in two subchapters, partly immersed and fully submerged hydrofoil. The first one presents results for hydrofoil submerged to the draught $h = 35$ cm. An analysis covered a total number of 68 simulation runs of which 44 are presented. Simulations were made for attack angled 5 to 30 degrees. In order to present results in a more efficient way, a decision was made to show results for 10, 20 and 30 degrees only.

In the first section of this subchapter, results are presented for all three used materials of Model 1, all three angles of attack and speeds except for simulations with composite materials (Model1c) and Model 2. Results for simulations of Model1c and Model 2 are presented for 10 and 20 degrees for inflow speed of 2 m/s because for bigger attack angle and inflow speeds deformations of the structural domain were too big to take validate results from them and for the sake of research they were discarded.

3.1. Results for immersed hydrofoil to the draft $h = 35$ *cm*

Example of distribution of deformation and stress results for Model1a can be seen in Figure 6. Values of deformation and stress as can be seen in Figure 7. and Figure 8. For attack angle of 30 degrees and inflow speed of 6 m/s largest deformation and stress has occurred, Figure 6. In case of inflow speed of 6 m/s and attack angle range between 10 to 20 degrees stress was 14.489 MPa while for attack angle range between 20 to 30 degrees stress was 7.5315 MPa. The drop of 51.9% was observed. Lower values of stress and deformation for the second rage of attack angle was in correlation with the drop in hydrodynamic pressure on hydrofoil for attack angle of 30 degrees, Figure 9. Observed physical phenomena were most noticeable in the case of partly immersed hydrofoil of structural steel. Mentioned can be related to a drop-in lift force after stall angle which can occur at attack angle of around 20 degrees.

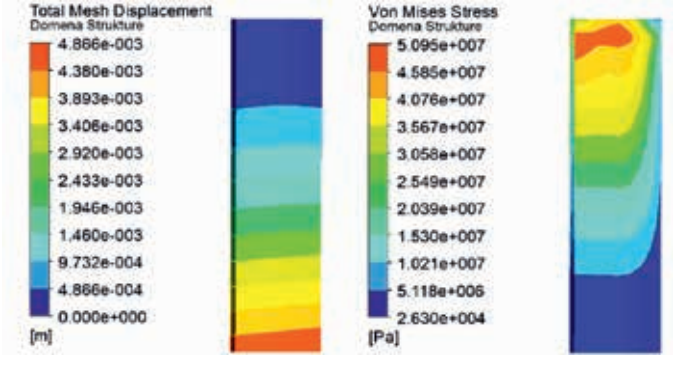

Figure 6: Distribution of deformation (left) and stress (right), results are presented for attack angle of 30 degrees and fluid inflow on the Model1a of 6 m/s

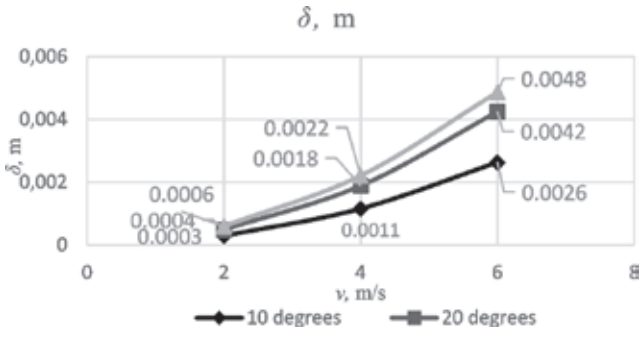

Figure 7: Deformation values of Model1a for h=35 cm

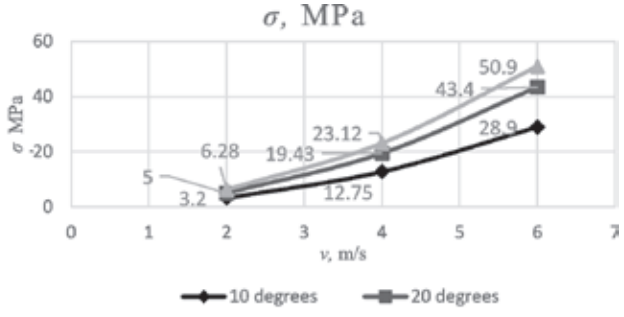

Figure 8: Stress values of Model1a for h=35 cm

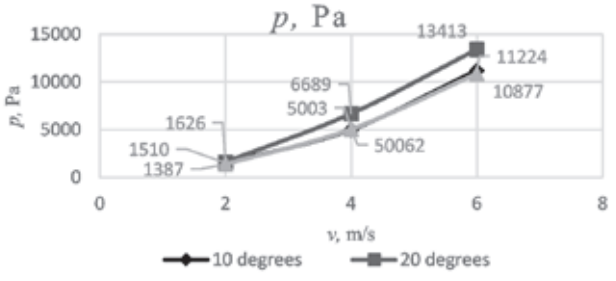

Figure 9: Representation of hydrodynamic pressure on hydrofoil surface of Model1a

In the case of the Model1b, similar results have occurred. Based on the material properties of aluminium Table 1, it was predictable that deformations and stress values will be higher compared to values for stainless steel. Simulation results in form of deformations, Figure 10. and stress, Figure 11. of *Model1b* are interdependent.

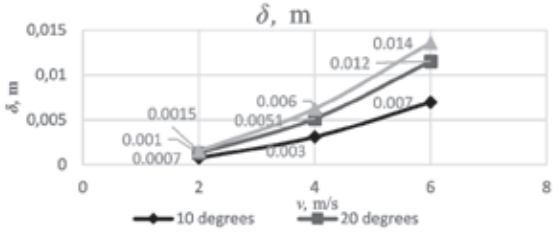

Figure 10: Deformation values of Model1b for h=35 cm

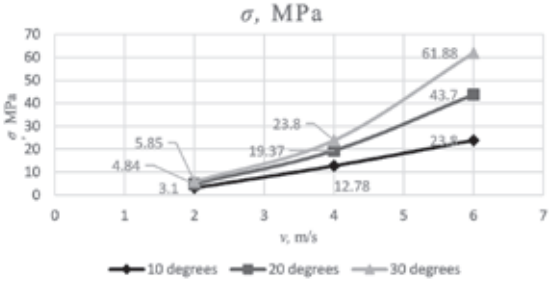

Figure 11: Stress values of Model1b for h=35cm

Model1c didn't withstand hydrodynamic load as Model1a and Model1b, as expected. Due to extremely large deformations of Model1c and Model 2 validate results are taken and presented only for attack angles of 10 and 20 degrees for inflow speed of 2 m/s. Reviewing the result, Figure 12. and Figure 13. it can be concluded that Model 2 has better characteristic of Model1c. Model 2 still couldn't withstand higher load conditions in operational case when inflow speed was 4 m/s.

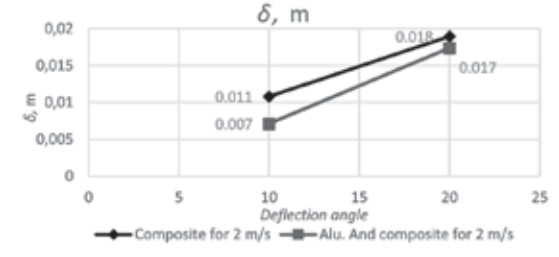

Figure 12: Deformation values of Model1c and Model 2 for h=35 cm

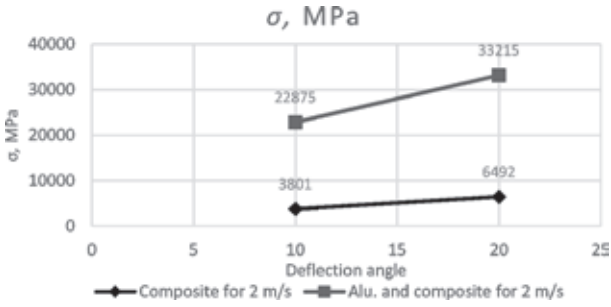

Figure 13: Stress values of Model1c and Model 2 for h=35 cm

3.2. Results for fully immersed hydrofoil

For fully immersed hydrofoil data representation order is same as for partly immersed hydrofoil. Within Figure 14. deformation distribution along the hydrofoil wing is represented along with stresses. Maximal values from Figure 14 can be seen in the diagrams in Figures 15. and Figure 16.

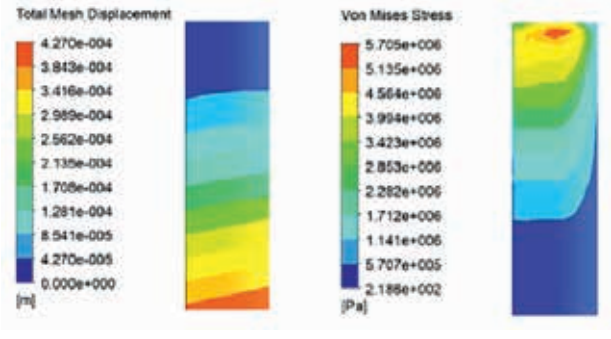

Figure 14: Distribution of deformation (left) and stress (right), results are presented for attack angle of 10 degrees and fluid inflow of 2 m/s, for Model1a

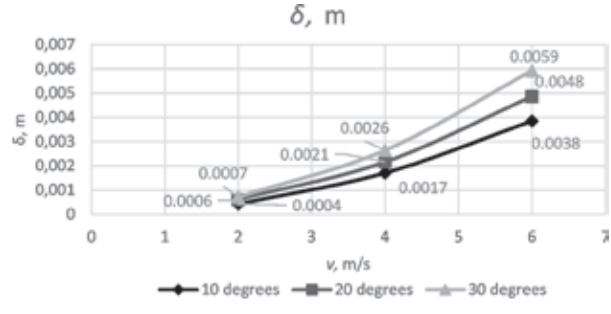

Figure 15: Deformation values of fully immersed Model1a

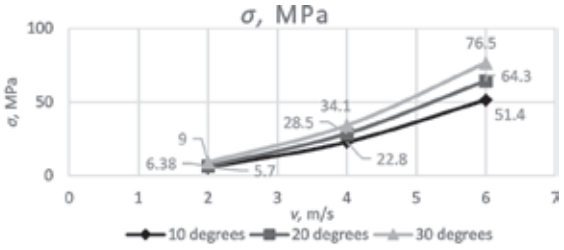

Figure 16: Stress values of fully immersed Model1a

Values of fully immersed hydrofoil with material properties of stainless steel (Model1a) are presented in Figure 15, Figure 16. As can be seen, all deformations are in elastic region with maximum deformation of 5,9 mm and maximum stress of 76.5 MPa. Based on results, stainless steel was recognized as most robust material. With maximum deformations of 18 mm, Figure 18, hydrofoil with aluminium properties (Model1b) can be used for the same operation load because stresses are still in elastic area with a maximum value of 81.08 MPa, Figure 18. This maximum value was obtained in conditions that were not meant to happen in conventional operations of hydrofoils because of the fact that after stall angle of around 20 degrees lift force start to decrease and hydrofoils are not useful.

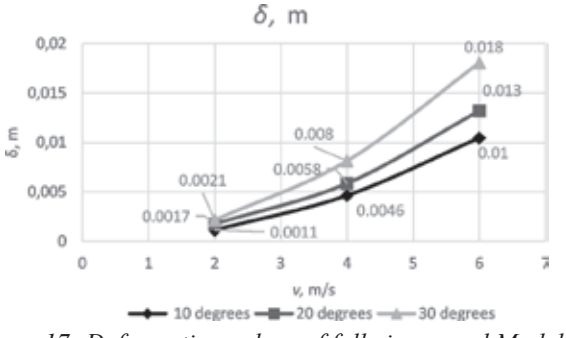

Figure 17: Deformation values of fully immersed Model1b

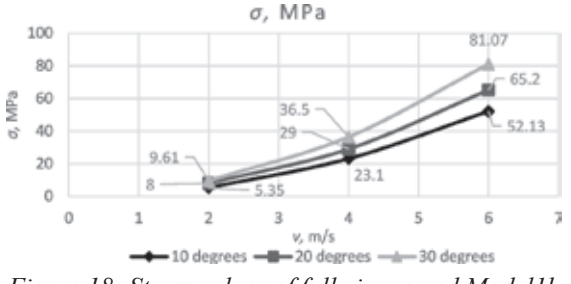

Figure 18: Stress values of fully immersed Model1b

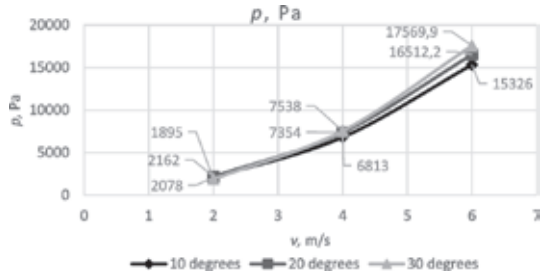

Figure 19: Hydrodynamic pressure values on surface of fully immersed Model1b

Results for Model1c and Model 2 can be seen in Figure 20. and Figure 21. Model with additional stiffener has shown better characteristic in a case of fully immersed hydrofoil based on deformation values.

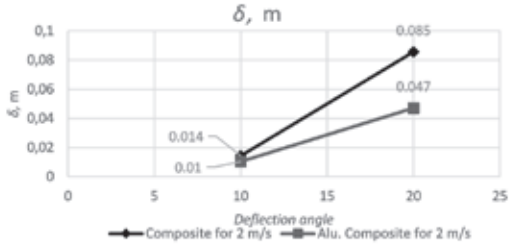

Figure 20: Deformation values of fully immersed Model1c, composite and Model 2

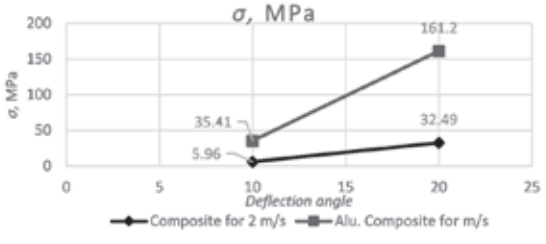

Figure 21: Stress values of fully immersed Model1c, composite and Model 2

Composite used in this research didn't come close to material properties of aluminium and stainless steel and with that cannot be used in the same load conditions, Figure 22. Whit usage of additional stiffener which was added on Model 2 deformation values were lowered, Figure 22, compared to Model1c. Model 2 has endured higher stress values because of local stress in additional stiffener, Figure 23.

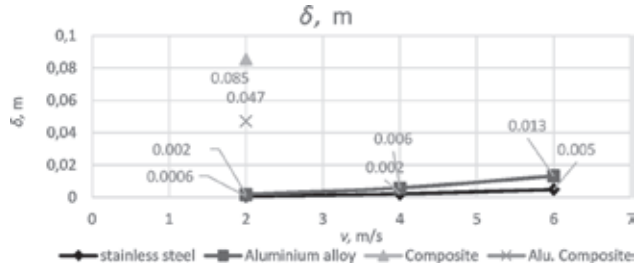

Figure 22: Comparison of largest deformation values for all tested materials (Model1a, Model1b, Model1c, Model 2)

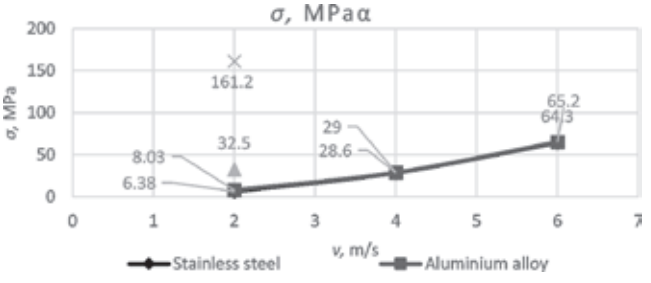

Figure 23: Comparison of largest stress values for all tested materials (Model1a, Model1b, Model1c, Model 2)

4. Conclusion

In order to adjust stiffness, deformations, and stresses two different 3D geometry models of hydrofoils were investigated in a steady flow. Simulations were run for three different material properties, which were stainless steel, aluminium, and composite. Main variables were attack angle and inflow fluid speed. Attack angle was altered for simulations between three angle values which were 10, 20 and 30 degrees and inflow speeds were 2, 4 and 6 m/s. Two-way fluid-structure interaction analysis was used with which *FEM* and *CFD* software's were combined in one analysis. A total of 68 simulation runs were performed and results are presented for 44 numerical simulations. First of all, during this research 15 simulations were performed in order to optimize analysis settings and fluid domain size.

Presented research tried to explore and expand knowledge about the behavior of hydrofoils in various load conditions, check for stiffens criteria based on same load conditions and inspect the behavior of composite material regarding the way in which stiffener could be applied.

Results have shown that the stainless steel (Model1a) and aluminium (Model1b) hydrofoils for full and partially immersed cases have similar hydrodynamic behavior,

except that rations between deformation and stress values of 10 to 20 and 20 to 30 degrees were different for immersed and fully submerged hydrofoils. For partly immersed hydrofoils attack angles, after stall angle, values show slower growth of deformation and stress values. Observed phenomena can be explained with decrease of lift force after around 18 to 20 degrees of attack angle. As a conclusion, hydrofoils with both material properties can be used in tested operational conditions.

Tested combination of aluminium and composite material (Model 2) can withstand load conditions to attack angle of 20 degrees and inflow speed of 2 m/s. Composite hydrofoil performance (Model1c), such as can be improved with additional stiffeners as can be seen on example with Model 2 results. In a process of designing composite hydrofoil with stiffener, a suggestion would be to place stiffener in the center of the wing. As a remark for further research free surface conditions, which were discounted in the presented simulations should be checked, in order to investigate drop in deformation and stress values for partly immersed hydrofoil.

Acknowledgements

This research was carried out within the project *uniri-technic-18-159* (*Development of Methodology for Ship Design and Production towards Industry 4.0. Concept)* funded by the University of Rijeka support research program.

References

1. Tayfun E. Tezduyar,Takizawa K., Moorman C., Samuel Wright S., Christopher J. (2010) Multiscale sequentially-coupled arterial FSI technique, Computational Mechanics Volume 46, Issue 1, pp 17–29,
2. Yuri, B., Kenji, T. and Tayfun, E. T. (2013) Computational Fluid-Structure Interaction, Methods and Applications, A John Wiley & Sons, Ltd., Publication,
3. Liaghat T., Guibault F., Allenbach L., and Nennemann B. (2014) Two-way fluid-structure coupling in vibration and damping analysis of an oscillating hydrofoil, Department of Mechanical Engineering - Polytechnique Montreal
4. Hutchison, S.R. (2012) Numerical Modelling of Hydrofoil Fluid-Structure Interaction, University of Tasmania
5. Schmucker, H., Flemming, F. and Coulson, S., (2010) Two-way coupled fluid structure interaction simulation of a propeller turbine. IOP Conference Series: Earth and Environmental
6. Gustavo, A. Z., Paul B, Bryce W. P. Andrew P. (2014) Experimental study of the steady fluid solid interaction of flexible hydrofoils, Journal of Fluids and Structures 51
7. P.A. Brandner and B.W. Pearce, Experimental Modeling of Steady Hydrofoil Fluid-Structure Interface, Australian Maritime College, (2019) Cavitation aggressiveness on hydrofoil
8. Carrat J.B., Bouvard T., Fortes-Patella R., Franc J. P. (2019) Cavitation aggressiveness on a hydrofoil, Conference series: Earth and Environment science
9. Harwood C.M. (2016) The Hydrodynamic and Hydroelastic Responses of Rigid and Flexible Surface-Piercing Hydrofoils in Multi-Phase Flows, A dissertation submitted in partial fulfillment of the requirements for the degree of Doctor of Philosophy, The University of Michigan
10. Young, Y., and Brizzolara S. (2013), Numerical and physical investigation of a surface piercing hydrofoil, in Proc. Third. Intl. Symp. Marine Propulsors
11. ANSYS, Inc (2013), ANSYS Mechanical User's Guide, Published in the U.S.A,

12. Swales, P., A. Wright, R. McGregor, and B. Cole (1973), Pressure, flow visualization and ventilation, *Hovering Craft and Hydrofoil*, *13* (1), 11–16.
13. Swales, P., A. Wright, R. McGregor, and R. Rothblum (1974), Mechanism of ventilation inception on surface piercing foils., *Journal of Mechanical Engineering Science*, *16* (1), 18–24.
14. Rothblum, R. S., D. A. Mayer, and G. M. Wilburn (1969), Ventilation, cavitation and other characteristics of high speed surface-piercing strut, *Tech. Rep. 3023*, Naval Ship Research and Development Center.
15. Waid, R. L. (1968), Experimental investigation of the ventilation of vertical surface-piercing struts in the presence of cavitation, *Tech. Rep. AD0738493*, Naval Ship Research and Development Center.
16. Zamarin A., Rudan S., Plenča S., (2018) Collision simulation of composite patrol high-speed craft, 23 Symposium on Theory and practice of shipping, SORTA
17. ITTC (2002), *Ittc international towing tank conference catalogue of facilities: towing tanks, seakeeping and manoeuvring basins, circulating water channels, cavitation tunnels*, International Towing Tank Conference.
18. Bungartz, H.; Schäfer, M., (2006) Fluid-structure Interaction: Modelling, Simulation, Optimization. Springer-Verlag,